

# **Parametric Dependence in Model Epidemics. I: Contact Related Parameters.**

(IN PRESS, *JOURNAL OF BIOLOGICAL DYNAMICS*)

W. M. Schaffer<sup>1,2</sup> and T. V. Bronnikova<sup>1</sup>

1. Department of Ecology and Evolutionary Biology
  2. Program in Applied Mathematics
- The University of Arizona  
Tucson, Arizona 85721

**Keywords:** Bifurcations, Continuation, Epidemiology, Mathematical models, SEIR Equations.

**Mathematical Subject Classification Codes:** 37M05, 37M20, 65P20, 65P30, 92D30.

**Abstract.**

One of the interesting properties of nonlinear dynamical systems is that arbitrarily small changes in parameter values can induce qualitative changes in behavior. The changes are called bifurcations, and they are typically visualized by plotting asymptotic dynamics against a parameter. In some cases, the resulting bifurcation diagram is unique: irrespective of initial conditions, the same dynamical sequence obtains. In other cases, initial conditions *do* matter, and there are coexisting sequences. Here we study an epidemiological model in which multiple bifurcation sequences yield to a single sequence in response to varying a second parameter. We call this simplification the emergence of *unique parametric dependence* (UPD) and discuss how it relates to the model's overall response to parameters. In so doing, we tie together a number of threads that have been developing since the mid-1980s. These include period-doubling; subharmonic resonance, attractor merging and subduction and the evolution of strange invariant sets. The present paper focuses on contact related parameters. A follow-up paper, to be published in this journal, will consider the effects of non-contact related parameters.

## Introduction.

Dynamical systems [1] are mathematical objects used to model the time evolution of real world systems. In real-world applications, one distinguishes *system* from *environment*. Then the time evolution of the system is determined jointly by internal feedback and the state of the environment, while the environment, which may or not be variable, is unaffected by the system (Figure 1).

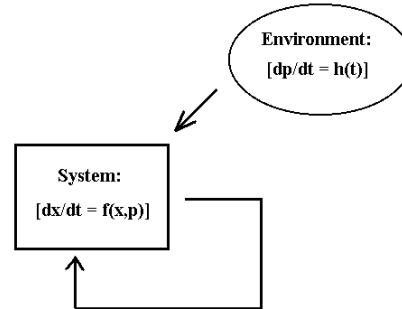


**Figure 1.** The time evolution of a dynamical system is determined by internal processes and the environment.

Consider, for example, ordinary differential equations of form

$$\begin{aligned} \dot{\mathbf{x}} &= \mathbf{f}(\mathbf{x}, \mathbf{p}) \\ \dot{\mathbf{p}} &= \mathbf{h}(t) \end{aligned} \quad (1)$$

Here,  $\mathbf{x}$ , which may be vector-valued, is the *state of the system*, the quantity or quantities that “evolve” according to the processes at hand. Correspondingly,  $\mathbf{p}$ , which may also be vector-valued, is the *state of the environment* as represented by parameter values.

The system-environment dichotomy<sup>1</sup> motivates complementary approaches to studying dynamics. On the one hand, one can fix parameter values and study the evolution of the state variables,  $\mathbf{x} = \{x_1, \dots, x_n\}$ . Conversely, one can map out regions of parameter space corresponding to different dynamical regimes. In the first case, one works in the *phase space*, which is a vector space, the axes of which are the values of the state variables. In the second case, one works in *parameter space*. Sometimes, one does a bit of both and plots one of the state variables, or a measure of all them, for example, their Euclidean norm, against the value of a parameter. The resulting construction is called a *bifurcation diagram*.

In the present paper, we utilize all three approaches to investigate the dynamics

<sup>1</sup> While straightforward in principle, distinguishing system from environment can be difficult in practice. The problem can be especially vexing when one is dealing with systems in nature, as opposed to the controlled conditions of the laboratory.

of a well-studied model of childhood epidemics. In the course of this investigation, we describe the emergence of *unique parametric dependence* (UPD), by which we mean the existence of a single bifurcation diagram that is independent of initial conditions. UPD implies *global stability* [1] over a range of parameter values and, in the non-trivial case, a unique sequence of bifurcations.

### SEIR Models of Microparasitic Infections.

SEIR equations categorize host individuals (Figure 2) with regard to disease status: **S**usceptible, **E**xposed (but not yet infectious), **I**nfectious and **R**ecovered (and immune). As such, they assume that individuals are either infected or not – *i.e.*, the concept of *parasite load* [2, 3] does not enter. They further presume that recovered individuals never re-enter the **S**usceptible class, for which reason they are used to model infections such as measles, mumps and rubella, in which a single exposure typically confers life-long immunity.

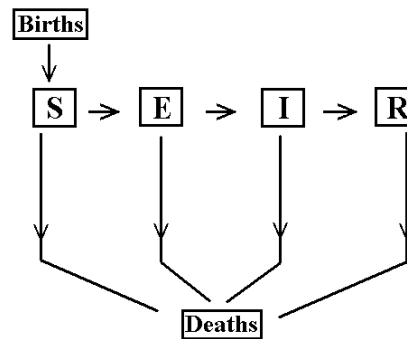


**Figure 2.** SEIR model of microparasitic infections. Individuals enter the **S**usceptible class at birth and progress to become **E**xposed, **I**nfectious and **R**ecovered.

The boxes and arrows in Figure 2 can be implemented in various ways. In the present paper, we work with ordinary differential equations. We further assume

1. *Constant* host population size;
2. *Quadratic* transmission, *i.e.*, the rate at which **S**usceptibles enter the **E**xposed class is proportional to the product,  $S \times I$ ;
3. *Linear* transition between the remaining categories, *i.e.*, the rates at which individuals enter the **I**nfectious and **R**ecovered classes are respectively proportional to  $E$  and  $I$ .
4. *Seasonal variation* in transmission - the so-called "school year effect" [4], which we model as a simple trigonometric function.

Translating these assumptions, all of which do admitted violence to biological

reality ([5- 8] and below), into mathematics yields

$$\begin{aligned} \dot{S} &= m(N - S) - B(t)SI; & \dot{E} &= B(t)SI - (m + a)E \\ \dot{I} &= aE - (m + g)I; & B(t) &= B_0(1 + \varepsilon_B \cos 2\pi t) \end{aligned} \quad (2)$$

Here,  $N$  is the total number of hosts;  $m^{-1}$ , the mean host longevity;  $a^{-1}$ , the mean latency period,  $g^{-1}$ , the mean period of infection, and  $B(t)$ , the time-varying contact rate. Note that the assumption of constant population size removes a degree of freedom, thereby obviating the need for an equation for  $dR/dt$ .

Often [9], Equations (2) are partially non-dimensionalized by setting

$$\begin{aligned} s &= S / N; & e &= E / N \\ i &= I / N; & \beta_0 &= B_0 N \end{aligned} \quad (3)$$

Then

$$\begin{aligned} \dot{s} &= m(1 - s) - \beta(t)si; & \dot{e} &= \beta(t)si - (m + a)e \\ \dot{i} &= ae - (m + g)i; & \beta(t) &= \beta_0(1 + \varepsilon_B \cos 2\pi t) \end{aligned} \quad (4)$$

## Methods.

The results presented here were obtained by numerical integration of the differential equations and by continuation of periodic itineraries and the bifurcation points of Poincaré maps constructed therefrom. The latter were obtained by sampling solution curves of log-transformed versions of Eqs (4) at time intervals equal to the period of forcing, which was one year. To facilitate comparison with the work of Schwartz and his associates [10-13], parameters were set to the following values:  $a = 100$ ;  $g = 35.84$ ;  $m = .02$ ;  $\beta_0 = [0, 3000]$ ; and  $\varepsilon_B = [0, 1]$ .

Forward bifurcation diagrams (Figures 3, 7) on what we call the *main period-doubling sequence* were computed in the usual way [14], with the state variables initially, *i.e.*, for  $\varepsilon_B = 0$ , set to the equilibrium values that obtain absent seasonality. Reverse main sequence diagrams (Figures 3 and 7) were initialized with points on the  $\varepsilon_B = 1$  attractor computed from the corresponding forward diagrams.

Chaotic saddles (Figure 4) were visualized as prescribed by Rand and Wilson [15]. In detail, trajectories initiated within one or more small cubes surrounding an attractor were followed until re-entering the cube.<sup>2</sup> From the data thus generated,  $T$ -recurrent points, *i.e.*, points that recur within a specified  $\varepsilon$  after  $T$  simulated years, were identified. Newton-Raphson root finding [16] was then used to locate nearby periodic orbits, the stability of which was determined via the calculation [14] of Floquet multipliers. Points on the stable orbits were used to initialize forward and backward bifurcation diagrams for coexisting resonances (Figures 3, 5, 7).

Periodic orbits were continued [17] – typically against  $\varepsilon_B$ , *e.g.*, Figure 10 – using secant prediction and chord-Newton correction with adaptive step control. As described in [18-20], the required Jacobian matrices were computed using concurrent integration of the equations of first variation. This allowed us to follow cycles of long period. Saddle-node and period-doubling bifurcations on the continuations were identified by application of standard [17, 21] criteria. Continuation of these bifurcations in the  $B_0$ - $\varepsilon_B$  plane yielded the bifurcation curves shown in Figures 8 and 9. By way of contrast, boundary and interior crises (Figure 8) were identified by brute force inspection of forward and backward bifurcation diagrams.

### Autonomous Dynamics.

In the absence of seasonality, *i.e.*, when  $\varepsilon_B = 0$ , Equations (4) manifest equilibrium dynamics [9]. More precisely, there are two equilibria. The first is the “no-disease” state,

$$(s^0, e^0, i^0) = (1, 0, 0); \quad (5)$$

the second, the *endemic* state, which is given by

$$(s^*, e^*, i^*) = \left( R_0^{-1}, \frac{m}{m+a}(1 - R_0^{-1}), \frac{am}{(m+g)(m+a)}(1 - R_0^{-1}) \right) \quad (6)$$

Here,

---

<sup>2</sup> Values of  $(S_0, I_0)$  were chosen on  $[S_{\min}, S_{\max}]$  and  $[I_{\min}, I_{\max}]$ ; values of  $E_0$ , from the approximation,  $E \approx [(m+g)/a]I$  [10].

$$R_0 = \frac{a\beta_0}{(m+a)(m+g)} \quad (7)$$

is the basic reproductive rate [9, 22] of the disease, essentially the number of secondary infections that result from a single contagion.

With  $R_0 < 1$ , the no disease equilibrium is stable, and the disease dies out. Correspondingly, with  $R_0 > 1$ , it is the endemic state that is stable, and the disease persists. Locally, there is a *transcritical bifurcation* at  $R_0 = 1$ , at which point the equilibria collide and exchange stability. More generally, it can be shown [23, 24] that, with  $R_0 > 1$ , the endemic state is *globally stable* on  $\Omega = \{(s, e, i) \in \mathbf{R}^3 \mid s, e, i \geq 0; s + e + i \leq 1\}$ . This is an extension of a corresponding result first proved by Lajmanovich and Yorke [25] for *SI* models. For somewhat larger values of  $R_0$ , two of the three eigenvalues complexify, and there are damped oscillations. Note that because  $a \gg m$  and  $g \gg m$ ,

$$R_0 \approx \frac{\beta_0}{g}, \quad (8a)$$

and the “small” parameter (see below),

$$\varepsilon = \beta_0 i^* = \mu(R_0 - 1) \approx m \left( \frac{\beta_0}{g} - 1 \right) \quad (8b)$$

[10].

### Non-autonomous Dynamics.

With the addition of seasonality, Equations (4) manifest a wide range of dynamics. These include annual cycles – the simplest response to seasonal forcing – and modulations thereof, multi-annual cycles and transient and asymptotic chaos. Some of these behaviors are shown in Figure 3 ( $\beta_0 = 1500$ ), wherein the asymptotic dynamics – as indexed by  $\log I$  – are plotted against the magnitude of seasonality,  $\varepsilon_B$ . Regarding this picture, we note the following:

1. There is a *main period-doubling sequence* (MPD) first described by [11] whereon annual cycles gives way to oscillations of period 2, 4, 8, ..., years. These motions bear the imprint of seasonality: the number of infectives peaks yearly, regardless of the overall period.

Additionally, the higher period cycles are all “biennial” in the sense that time series of infectives manifest alternating high and low years (Figure 2b). As pointed out by [11], this fact makes difficult the task of distinguishing such cycles from period-2 dynamics in the presence of noise.

2. In addition to the MPD attractors, there are *coexisting subharmonic resonances* (CSRs) first reported by [10]. Here, the mark of seasonality is absent. For oscillations with rotation number,  $\rho = 1/n$ , the number of infectives peaks once during the course of a cycle, the amplitude of which is typically larger than that of cycles on the main sequence (Figure 2a). Correspondingly, for oscillations with  $\rho = m/n$ ,  $m > 1$ , there are  $m$  peaks per period.<sup>3</sup> CSRs are the product of saddle-node bifurcations (SN), which generate pairs of cycles. Of these, one is always non-stable (the saddle), whereas the other (the node) is initially stable.
3. Like the annual cycle, the nodal CSRs undergo period-doubling to chaos [10]. The resulting chaotic attractors subsequently lose stability when they collide with their basin boundaries, which in each case is the stable manifold of the saddle cycle. These events are called *boundary crises* (BC) [27]. Thereafter, what was formerly an attractor persists as a *chaotic saddle* [12] to which nearby trajectories are attracted before veering off in the unstable direction.
4. As first reported by [28], there is a discontinuity in the main sequence (in Figure 3c at  $\varepsilon_B \approx 0.4$ ), at which point, the MPD attractor undergoes an abrupt increase in size. This event is called an *interior crisis* (IC) [27]. It results from collision of a main sequence attractor with the stable manifold of one of the chaotic saddles. What follows is incorporation of the saddle into the main sequence attractor, which causes a qualitative change in the character of MPD dynamics [28]. Prior to the IC, main sequence motions are modulations of the annual cycle. After the crisis, there is a mixture of yearly outbreaks and subharmonic motions of longer period (Figure 3d). Such mixtures are reminiscent of historical notifications for measles and rubella in North America [28] and elsewhere [29].

---

<sup>3</sup> Here  $n$  is the number of points on the cycle, and  $m$ , the number of  $2\pi$  radian rotations required to visit them all [26] when the motion is plotted in a suitable coordinate system such as the **S-I** plane. Strictly speaking,  $\rho$  is only defined for planar mappings, whereas Poincaré maps of Equations (4) are three-dimensional. To first approximation, however,  $E(t)$  and  $I(t)$  are linearly related [10, 11]. This justifies approximating the stroboscopic dynamics of Equations (4) as planar maps and the application thereto of two-dimensional constructs, such as rotation number.

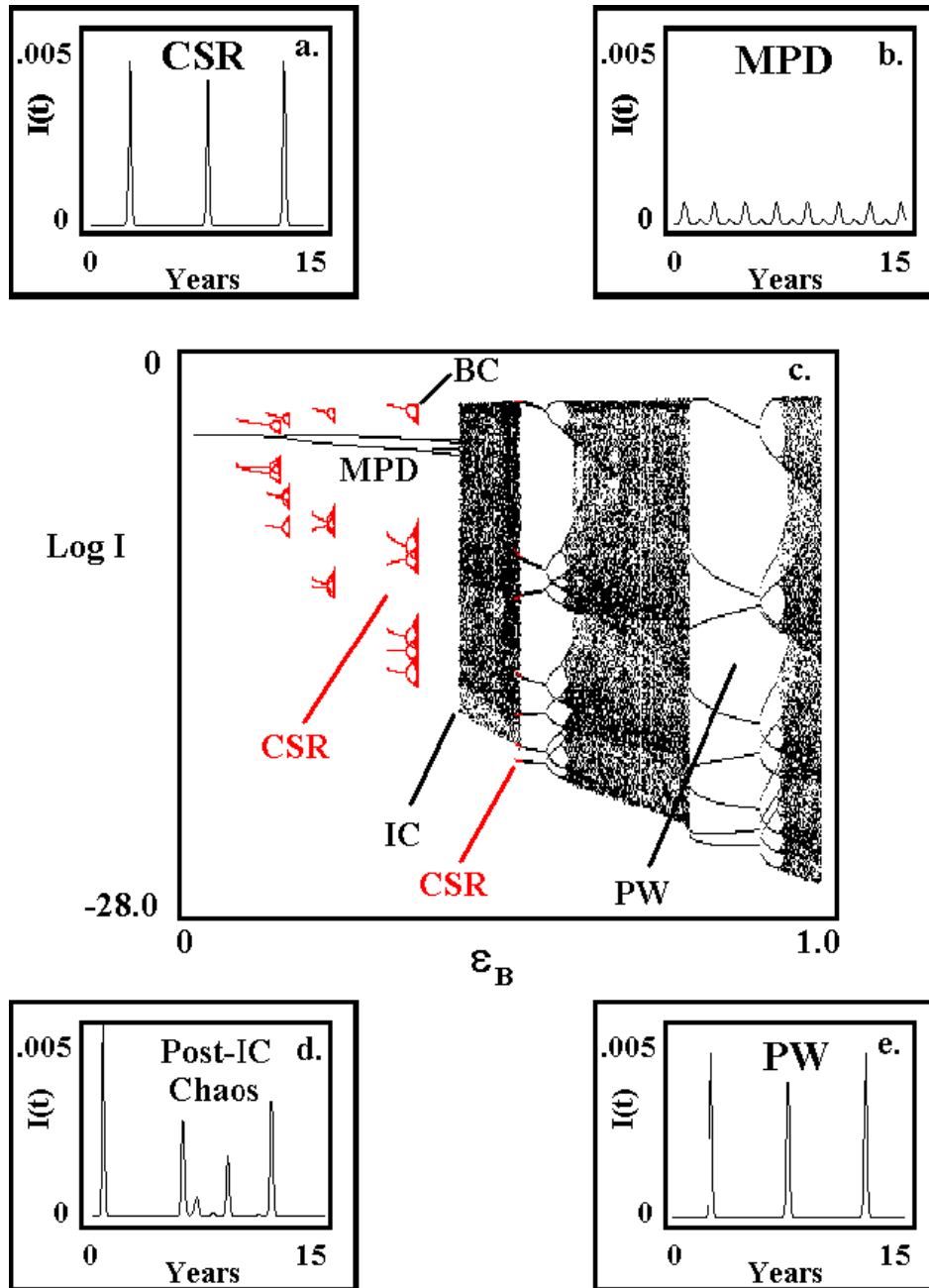


**Figure 3.** Complex dynamics in *SEIR* equations with  $m = .02$ ;  $a = 100$ ;  $g = 35.84$ ; and  $\beta_0 = 1500$ . Abbreviations as follows: **BC** = boundary crisis; **CSR** = coexisting subharmonic resonance; **IC** = interior crisis; **MPD** = main period-doubling sequence; **PW** = periodic window; **SN** = saddle node bifurcation. Only CSRs with first level Farey sequence rotation numbers,  $\rho=1/n$ , (see text below) are shown. **a.**, **b.**, **d.** and **e.** Representative time series. **c.** Bifurcation diagram (trajectories sampled stroboscopically). Coexisting attractors shown in red.

5. Following the interior crisis, the main sequence consists of dense bands punctuated by periodic windows (PW). The latter correspond to additional subharmonic resonances (Figure 3e) arranged in order of decreasing rotation number,  $\rho = m/n$ .

At first glance, Figure 3c suggests that the bifurcation diagram can be divided into two regions with coexisting bifurcation sequences to the left of the IC and a single sequence to the right. In fact, this is an oversimplification. As discussed below, the periodic windows to the right of the IC can manifest hysteresis, with the result that their associated resonances are partly on and partly off the main sequence. For example, in Figure 3c, period-7 oscillations coexist with the MPD just to the left of the PW.

### **Transient Chaos before the Interior Crisis.**

Collectively, the chaotic saddles produced by the destabilization of chaotic CSRs appear to constitute well-defined mathematical objects, sometimes referred to [30] as strange invariant sets (SIS). Like chaotic attractors, strange invariant sets are topologically transitive with the consequence that in the limit of infinite time, trajectories based at any point on a SIS pass arbitrarily close to every other point [31]. Rand and Wilson [15], who discovered such sets in the *SEIR* equations, called them "repellers." More accurately they are saddles. A visualization of one such SIS is shown in Figure 4a. Here,  $10^4$  trajectories were initialized within a small region (the red box) surrounding the main sequence attractor (an annual cycle) and terminated either after exceeding a predetermined number of steps or upon re-entering the neighborhood wherein they were initiated. Even though all such orbits eventually re-enter the box and approach the main sequence attractor, some of them shadow the SIS for extended periods. In short, coexistence of a SIS with a non-chaotic attractor makes possible chaotic transients, which, depending on the particulars, can be arbitrarily long [32]. This leads to the idea of "noise-stabilized chaos" [15]: in the presence of small perturbations, chaotic trajectories are observable absent the existence of a chaotic attractor. The critical point is that trajectories in the neighborhood of the non-chaotic attractor be temporarily attracted to the vicinity of the SIS before settling down to the asymptotic state. In the case of pre-vaccination outbreaks of measles [33], noise-stabilized chaos has been proposed [15] as an alternative to asymptotic chaos when realistic parameter estimates [7] place the system to the left of the IC (but see [34, 35]).

### Organization of the SIS.

Chaotic sets are sometimes described as being organized about "skeletons" of non-stable periodic orbits [36- 40]. By this it is meant that every point of a chaotic set is arbitrarily close to such an orbit [1, 31]. The Rand-Wilson "repeller" is no exception, the periodic orbits in question being the destabilized CSRs. To visualize a part of this skeleton, we identify *recurrent points* (Figure 4c) and color-code them by mean peak-to-peak interval,  $T_m$ , which is the inverse,  $\rho^{-1}$ , of the presumptive cycle's rotation number. The points so distinguished correspond to values of  $T_m$  ranging from 1 (dark red) to 14 (dark purple), and they include both the periodic orbits themselves and nearby pieces of their associated stable manifolds. In Figure 4d, we superpose the cycles, independently identified by Newton-Raphson root finding [16], with rotation numbers  $\rho = 1/3, 1/4, \dots, 1/14$ . As expected, each swatch of color is associated with a cycle. Moreover, there are two such cycles for each value of  $\rho$ , which observation is consistent with the fact that the CSRs are created in pairs.

We emphasize that the cycles identified in Figure 4d represent but a fraction of the periodic points about which the SIS is organized. Additional periodic orbits are created by period-doubling of the stable CSRs, as well as by periodic windows within the resulting chaotic regions (Figure 5d). In addition, there are periodic orbits called "ultra-subharmonics" [41] (Figures 5a, 5b) for which the rotation number is  $\rho = m/n$ , where  $m > 1$ . These cycles can be ordered according to the Farey sequence [26] (Figure 6), which is a scheme for approximating the real numbers by the rationals.

Like the  $\rho=1/n$  subharmonics, each ultra-subharmonic is the product of a saddle-node bifurcation with the initially stable cycle of each pair undergoing period-doubling to chaos (Figures 5c, 5d). Thereafter, the resultant chaotic attractors are destabilized by boundary crises. In short, we imagine that the SIS is densely populated by non-stable periodic orbits that can be sorted into a large, if not infinite, number of qualitative types corresponding to different values of  $\rho$ .

### Response to Varying a Second Parameter.

Next consider the consequences to the bifurcation diagram in Figure 3 of varying the mean contact rate,  $\beta_0$ . As shown in Figure 7, the principal effects are as follows:

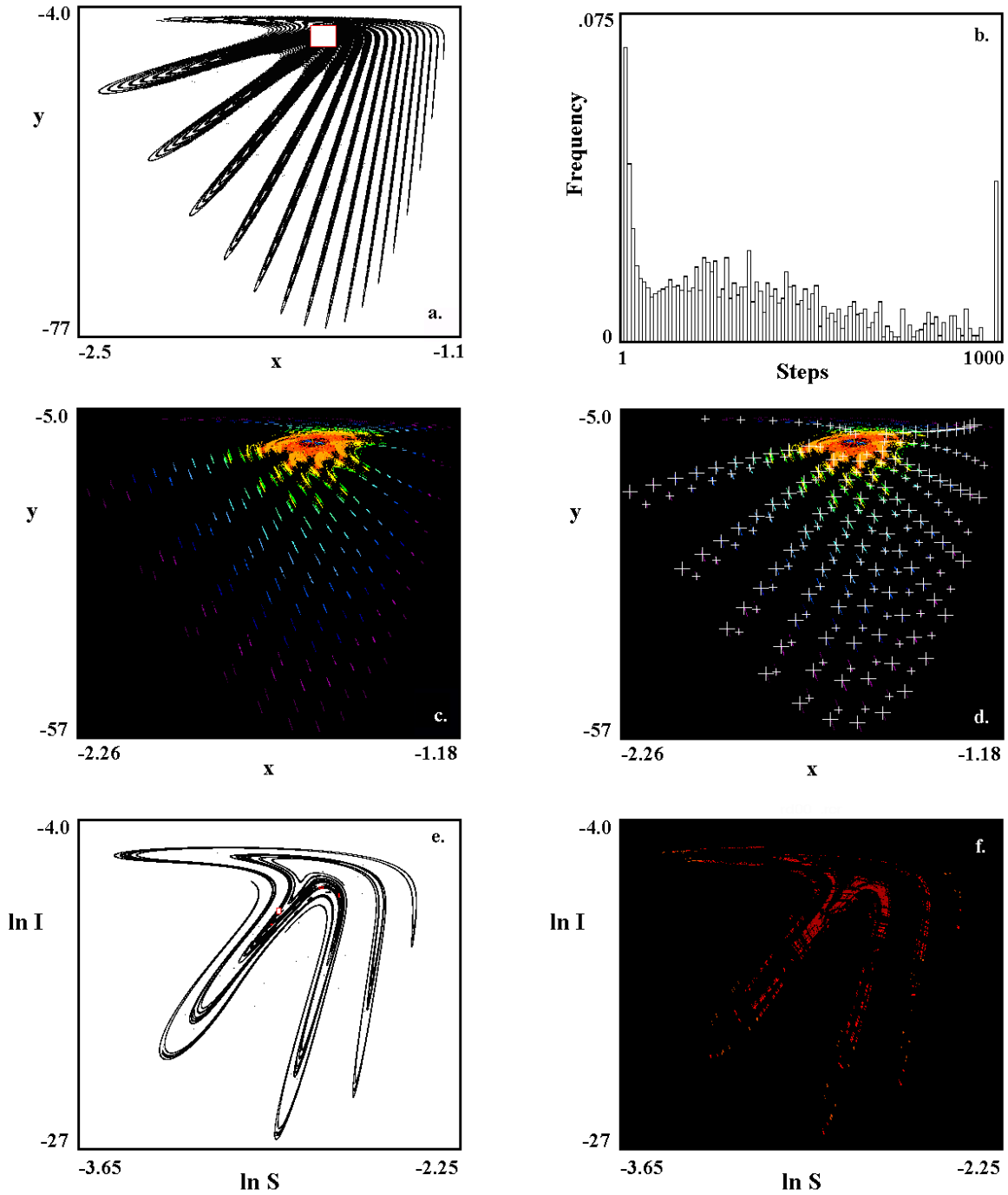


**Figure 4.** Non-stable chaos in log-transformed *SEIR* equations ( $x = \ln s$ ;  $y = \ln i$  and  $z = \ln e$ ). **a.-d.**  $\beta_0 = 500$ ;  $\varepsilon_B = 0.25$ . **e.-f.**  $\beta_0 = 1800$ ;  $\varepsilon_B = 0.27$ . Other parameters as in Figure 3. **a.** and **e.** The strange invariant set (SIS). **b.** Frequency distribution of trajectory lengths prior to re-entering cube of initial conditions (red box). For each initial condition, a maximum of 1000 steps were recorded **c.**, **d.** and **f.** Recurrent points color-coded by the mean peak-to-peak interval,  $T_m = \rho^{-1}$ , in the time series of infectives. Color-coding is by the visible spectrum (dark red:  $T_m=1$ ; dark purple:  $T_m=14$ ). **d.** Stable (large crosses) and unstable (small crosses) periodic points superposed on color-coded recurrent points.

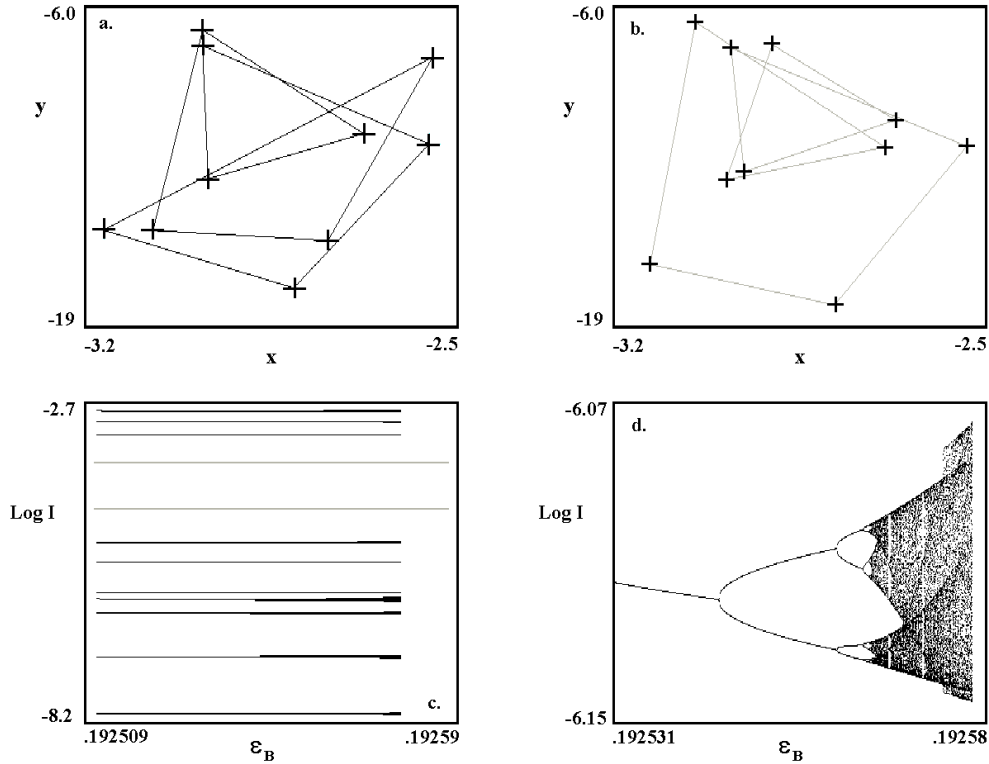


**Figure 5.** Ultra-subharmonic resonances ( $\beta_0 = 1800$ ;  $\epsilon_B = 0.27$ ) with rotation number  $\rho = 3/10$ . **a.** Nodal cycle **b.** Saddle cycle. **c.** The stable cycle undergoes period-doubling to chaos with increasing values of  $\epsilon_B$ . Coexisting period-2 cycle shown in gray. **d.** Magnification of **c.**

1. The MPD attractors undergo period-doubling. For sufficiently low values of  $\beta_0$ , the MPD is nothing more than a sequence of annual cycles (Figure 7a). For higher values of  $\beta_0$ ,
2. period-doubling kicks in, initially as a “bubble” (Figure 7b). Eventually, there emerges a small amplitude chaotic attractor.
3. The CSR bifurcation sequences also originate as “bubbles” – this can be seen in the case of the  $\rho=1/3$  resonance for  $\beta_0 = 800$  – and then move to the right. At the same time, the bubbles split into left and right halves (not shown), each delimited by a boundary crisis. With further increases in  $\beta_0$ , the right piece move quickly off the diagram at  $\epsilon_B = 1$ .

4. The left pieces also move to the right and, as they do, become incorporated (Figure 7b-d) into the main sequence as periodic windows. Incorporation *begins* when the boundary crisis that destabilizes a

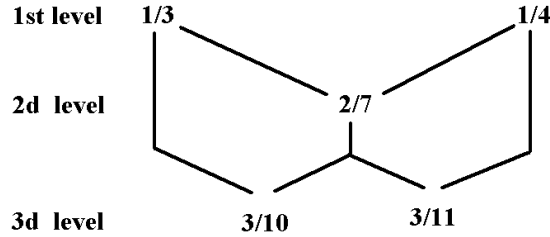


**Figure 6.** The first three levels of the Farey sequence between 1/3 and 1/4. The ordering can be continued downwards an infinite number of levels.

CSR coincides with the interior crisis and *concludes* when the generative saddle node bifurcation coincides with the IC. The first of these events is sometimes referred to as an attractor-merging crisis [42]; the second, as *subduction* [27]. Both are codimension-2 [17] bifurcations. For parameter values between them, the CSR bifurcation sequence is partly on and partly off the MPD. Thus, in Figure 7b, ( $\beta_0 = 1384$ ), the  $\rho = 1/8$  sequence has been partially incorporated into the MPD. Similarly, in Figure 7c ( $\beta_0 = 1900$ ), incorporation of the  $\rho = 1/4$  resonance has just begun, while incorporation of the  $\rho = 1/6$  resonances is complete. Between them, the  $\rho = 1/5$  resonance has partly joined the main sequence. Finally, in Figure 7d ( $\beta_0 = 2900$ ), incorporation of the  $\rho = 1/4$  bifurcation sequence is complete, but not that of the  $\rho = 1/3$  sequence. Between these sequences one observes a periodic window of  $\rho = 2/7$  ultra-subharmonics. Likewise, in Figure 7c, the  $\rho = 2/11$  PW is situated between the  $\rho = 1/5$  and  $\rho = 1/6$  windows.

5. With further increases of  $\beta_0$ , the region of large-scale chaos expands, while the erstwhile CSRs, now periodic windows on the MPD, continue to move to right and off the diagram (Figures 7c, 7d).

### Simplification of the SIS.

As its constituent CSRs join the main sequence with increasing values of  $\beta_0$ , the SIS that exists prior to the IC simplifies. More precisely, with incorporation of each CSR into the MPD, the SIS loses an infinite number of periodic orbits. The simplification is apparent if we compare the SIS that exists for  $\beta_0 = 500$  (Figures 4a-d) with the corresponding SIS for  $\beta_0 = 1800$  (Figures 4e, f). Whereas the former SIS includes recurrent points with rotation numbers down

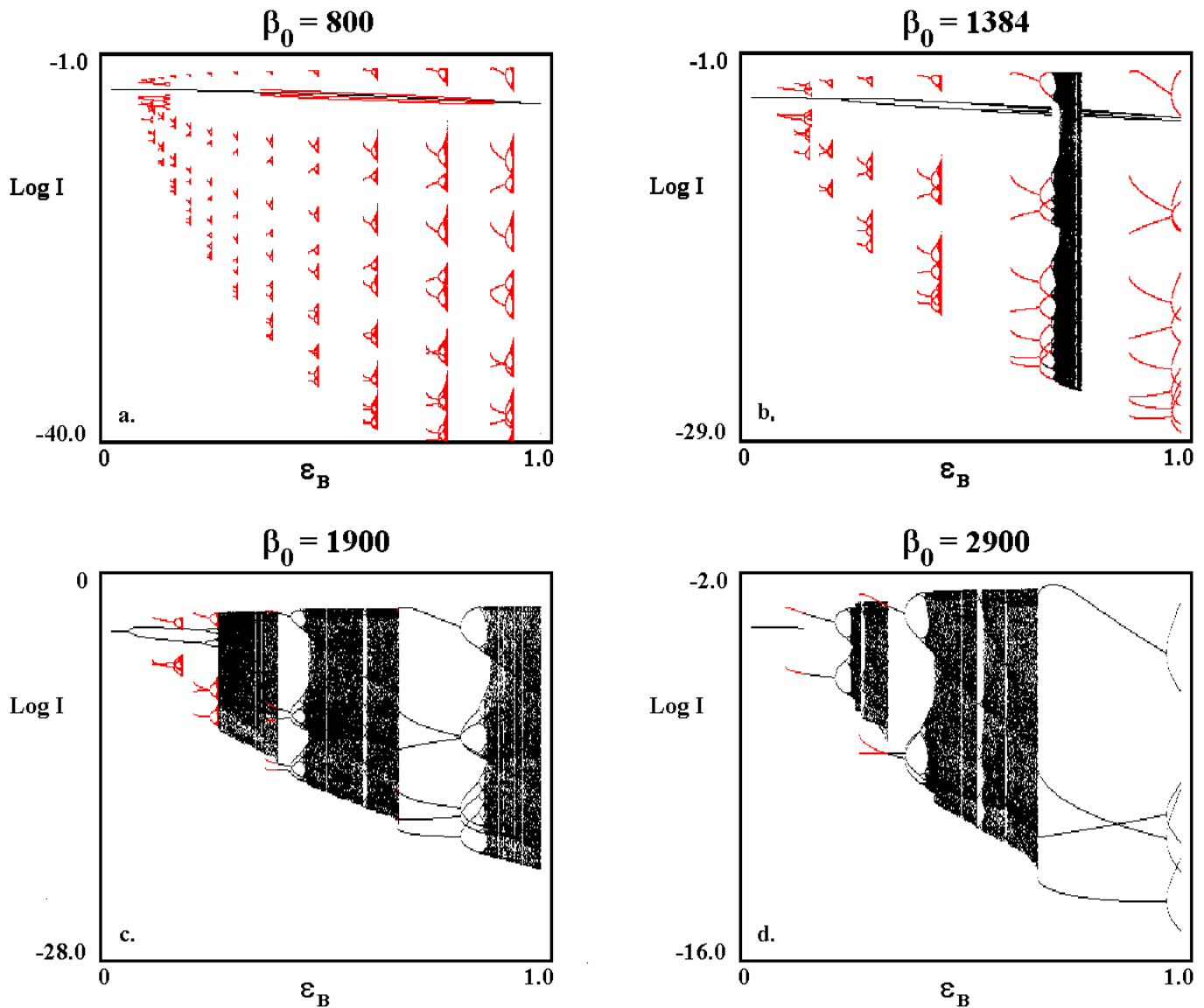


**Figure 7.** Response to varying the mean contact rate. **a.**  $\beta_0 = 800$ . Numerous CSRs coexist with the MPD, which is a sequence of annual cycles. The period-3 bifurcation sequence is a “bubble.” **b.**  $\beta_0 = 1384$ . The annual cycle on the MPD manifests period-doublings. The higher period CSR bifurcation sequences have moved off the diagram at the right. There is also a bubble of large-amplitude chaos on the MPD delimited by interior crises. **c.**  $\beta_0 = 1900$ . The  $\rho = 1/6$  and  $\rho = 1/5$  bifurcation sequences have joined the MPD, the latter only partly, while the  $\rho = 1/4$  and  $\rho = 1/3$  sequences remain off the MPD – the former just barely. The remaining CSRs have moved off the diagram. **d.** Of the CSRs in **a.**, only the  $\rho = 1/4$  and  $\rho = 1/3$  remain – the former having been entirely incorporated into the MPD, the latter only partly.

to  $1/16$ , the corresponding minimum in the second case is  $1/4$  - hence the ubiquitous shades of red corresponding to  $T_m = 2 - 4$  when one color-codes as in Figures 4c and 4d.

### Two Parameter Analysis.

The preceding observations motivate a two-parameter analysis [17, 34, 43, 44] wherein we delineate dynamical possibilities in the  $\beta_0\text{-}\varepsilon_B$  plane. (For an alternative, but related, approach, see [45].) Here we map out loci of period-doubling bifurcations on the MPD and the saddle-node bifurcations that give rise to representative CSRs. In the case of the MPD (Figure 8a), we show the first three period-doubling curves (PD-2, PD-4, PD-8) and the curve of interior crises.

Also shown is a curve period-2 saddle-node bifurcations (SN). Between this curve and PD-2, stable annual and biennial dynamics coexist [8, 34, 44]. As observed by [44], the point at which the curve of saddle-node bifurcations emerges from PD-2 is a codimension-2 bifurcation [17], at which juncture, the bifurcations on PD-2 change criticality [46].

Turning our attention to the CSRs, we map out curves of saddle-node bifurcations. These curves delimit regions in parameter space called *resonance horns* [26, 47], within which all periodic orbits have the same *reduced* rotation number,  $\rho_r$ , e.g., the reduced rotation of cycles with  $\rho = 2/4$  and  $\rho = 4/8$  is  $1/2$ .

In Figure 8b, we show the curve (SN) of saddle node bifurcations that delimits the  $\rho=1/3$  resonance horn and the first two period-doubling curves (PD) wherein the stable period-3 and period-6 cycles lose stability. Also shown is the curve of boundary crises (BC) that destabilize the period-3 chaotic attractor and the interior crisis curve (IC) noted above. Taken together, these curves divide the parameter plane into 3 regions. In region I, the period-3 bifurcation sequence is composed of CSRs, *i.e.*, it is entirely *off* the MPD; in region III, the sequence is contained entirely *within* the MPD where it appears as a periodic window. In region II, the sequence is *partly on* and *partly off* the MPD. This accounts for the incorporation process described above.

In Figure 8c, we display resonance horns ( $\rho=1/3$  to  $\rho=1/16$ ) for all the CSRs in Figure 7a ( $\beta_0 = 800$ ). Interestingly, the curves pile up at the left at  $\beta_0 \approx 200$ . This suggests a minimum value of  $\beta_0$  at which a large (infinite?) number of CSRs pop into existence. Increasing  $\beta_0$  beyond this value causes CSRs to drop out, one at a time, in order of decreasing rotation number, until at  $\beta_0 = 3000$ , there is only the  $1/3$  resonance.

The relationship of Figure 8 to the bifurcation diagrams in Figure 7 can be appreciated by fixing  $\beta_0$  and varying  $\varepsilon_B$  on  $[0,1]$ . Correspondingly, the

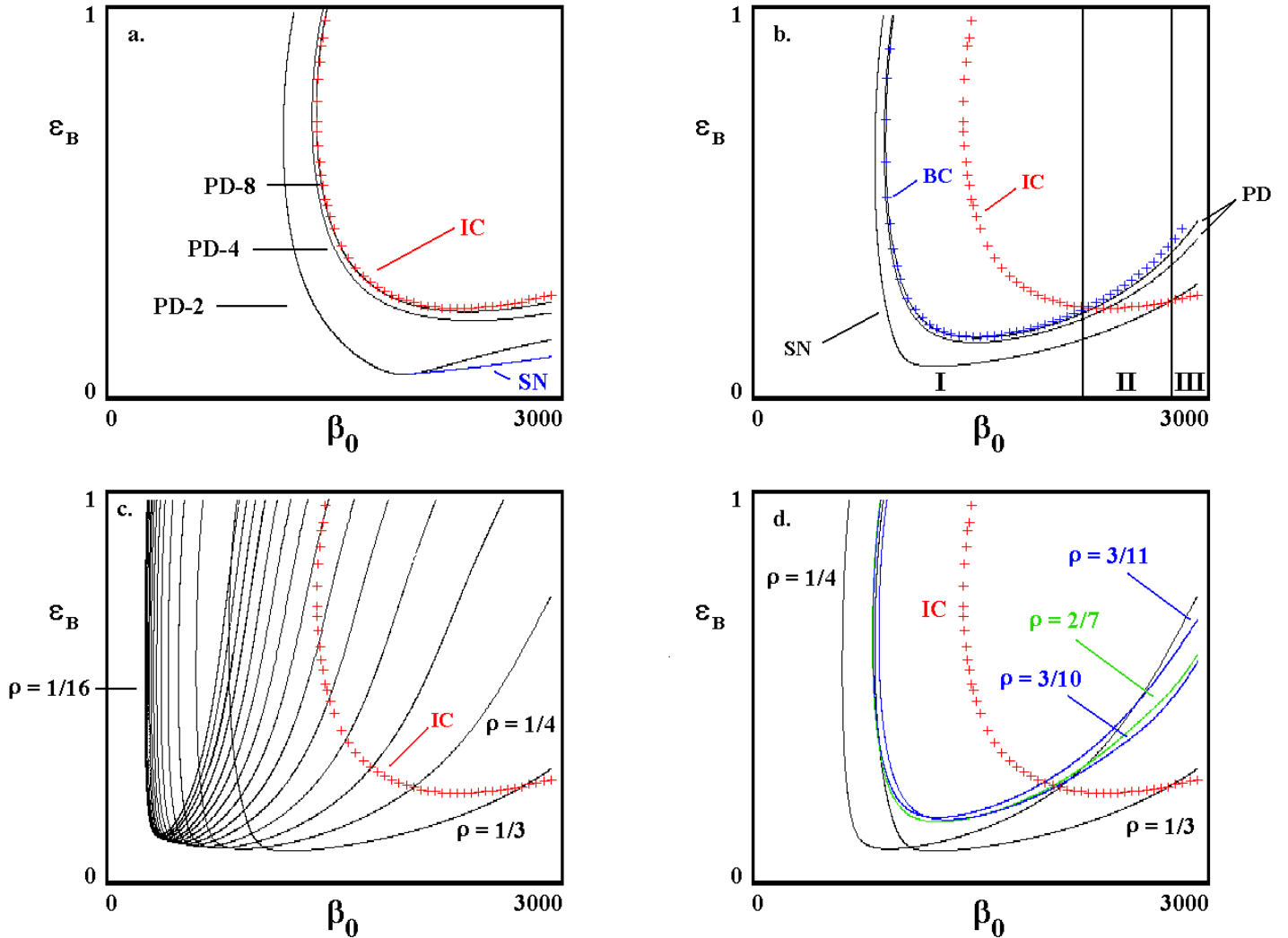


**Figure 8.** Two parameter analysis. **a.** Period-doubling bifurcations on the MPD. The first three bifurcations (PD-2, PD-4, PD-8) are shown. Also shown are the curve of interior crises (IC) and a curve of saddle-node bifurcations (SN) that produce period-2 orbits. Between SN and PD-2, stable period-2 dynamics coexist with the annual cycle. **b.** The  $\rho=1/3$  resonance horn. In addition to the curve of saddle node bifurcations, two period-doubling curves (PD) corresponding to period-6 and period-12 dynamics are shown. Also displayed is the boundary crisis curve (BC) whereat period-3 chaotic attractors are destabilized and the curve of interior crises (IC) on the MPD. Incorporation of the  $1/3$  resonance into the MPD begins at the BC-IC intersection and completes at the IC-SN intersection. This allows division of the parameter plane into the three regions discussed in the text. **c.** The  $\rho=1/3, \rho=1/4, \dots, 1/16$  resonance horns and the curve of interior crises. **d.** Ultra-harmonic resonance horns corresponding to the rotation numbers in Figure 6. First level resonances shown in black; second level, in red; third level, in green.

The relationship of Figure 8 to the bifurcation diagrams in Figure 7 can be appreciated by fixing  $\beta_0$  and varying  $\varepsilon_B$  on  $[0,1]$ . Correspondingly, the bifurcation sequences reported by [8] and [48] for a related model (see below) obtain *qualitatively* if one fixes  $\varepsilon_B$  and varies  $\beta_0$ .

It is worth observing that only a small number of resonances actually make it into the MPD. For the rest, the horns bend up too steeply to intersect the IC curve. Note that at moderate to high values of  $\beta_0$ , the curves sort out in order of decreasing values of  $\rho$  as one increases  $\varepsilon_B$ . Thus the order in which resonances appear in the bifurcation diagrams (Figures 3 and 7) accords with the Farey ordering in Figure 6.

Figure 8d completes our survey of resonance horns. Here we plot ultra-subharmonics corresponding to values of  $\rho$  between  $1/3$  and  $1/4$ . Like the  $1/3$  and  $1/4$  resonances, these cycles also intersect the IC curve and are incorporated into the MPD at higher values of  $\beta_0$  (Figures 7c, d).

## Discussion.

**A Global Perspective.** The present analysis extends previous investigations [2, 5-8, 12, 13, 15, 20, 22, 25, 28, 33-35, 43, 49-58] by offering an overall perspective on the remarkably variegated dynamics that obtain when a simple epidemiological model is subject to seasonal forcing. In so doing, we tie together a number of threads that have been developing in the epidemiological literature since the mid-1980s. As enumerated above, the relevant dynamical phenomena are the following:

1. Period-doubling to chaos, first reported by Aron and Schwartz [11], on the main sequence (MPD).
2. Subharmonic resonances (CSRs), first reported by Schwartz and Smith [10] (see also, [8, 45, 59]), that coexist with the MPD.
3. Strange invariant sets (SISs), first reported for Equations (4) by Rand and Wilson [15], which also coexist with the MPD.
4. Boundary crises, whereby CSRs are destabilized [10, 12] and become part of the SIS.
5. Interior crises whereby elements of the SIS are incorporated into the MPD [28].

The present analysis suggests that these phenomena are part of a unified whole:

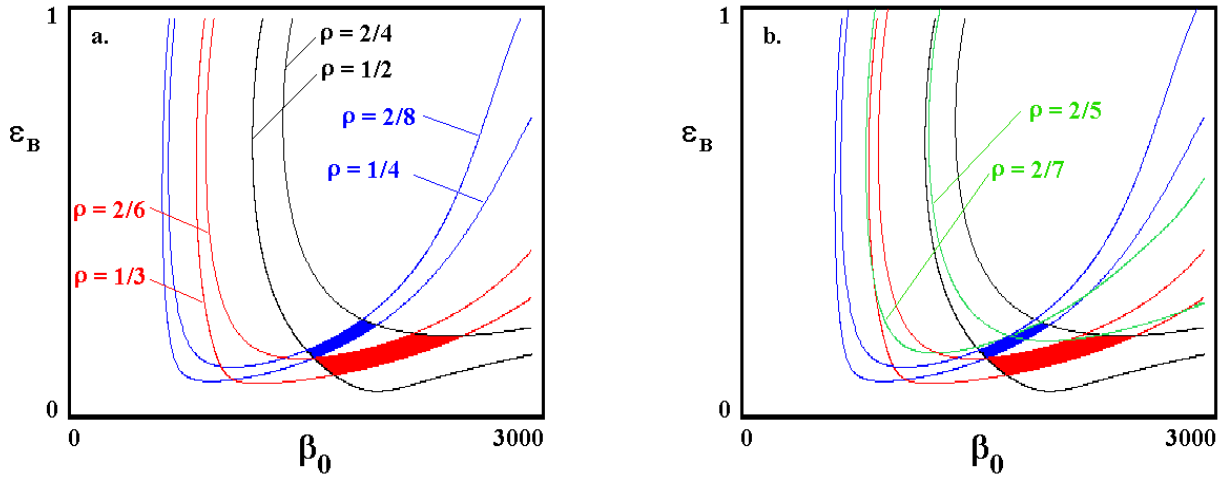
As parameters vary, periodic orbits are born, destabilized and become parts of chaotic attractors that themselves lose stability and join the SIS. The latter subsequently simplifies as its constituent saddles sequentially merge with the MPD.

Our results also make contact with bifurcation theory. As noted above, the BC-IC and SN-IC coincidences, *i.e.*, attractor merging [42] and subduction [27], that initiate and complete CSR incorporation into the MPD are codimension-2 bifurcations that can be studied with reference to homoclinic and heteroclinic connections [1, 60]. This suggests the possibility of higher codimension bifurcations that are the birthing place of the periodic windows [61] (see also, [62-64]).

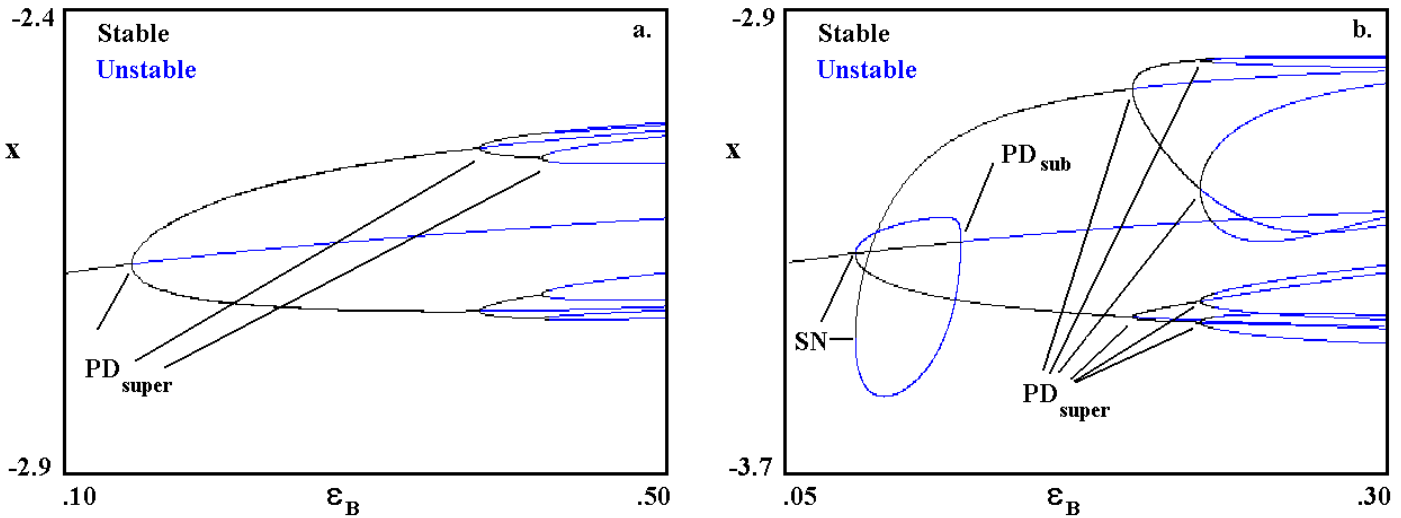
**Effects of Noise.** The present analysis is entirely deterministic, a simplification that limits its real-world applicability. Given finite population effects [58, 65], random forcing of disease systems in nature is inescapable, even in the absence of environmental change. Probably the most widely appreciated epidemiological consequence of noise is disease extinction [66-69] in small to moderate sized populations. But even in the absence of such “fade-outs,” stochastic forcing can have dramatic effects. Thus, with noise added to the dynamics, both stable CSRs and attractors on the MPD, as well as saddle cycles of the SIS, will be visited. There are other possibilities as well. One of these, reported by [13], is *bi-instability* (B-I), so-called because it involves two unstable cycles – for example, the period-1 oscillation, destabilized by period-doubling, and the saddle period-3 cycle. In this case, the unstable manifold of the period-3 cycle and the stable manifold of the period-1 cycle manifest heteroclinic crossings and a tangle (see [13], Figure 2). In the presence of stochastic forcing, B-I generates sustained dynamical complexity, and is therefore an alternative to noise-stabilized transient chaos on the SIS.

Figure 9a delineates the region in parameter space wherein period-3 B-I is the sole possible source of complex dynamics. Also shown is the corresponding region involving the unstable period-4 cycle. In Figure 9b, we do the same for the  $\rho = 2/5$  and  $\rho = 2/7$  ultra-subharmonics. Manifestly, these regions are close to those for which there are other sources of instability, with the result that distinguishing B-I from asymptotic and noise-stabilized chaos in nature may be difficult.

Like noise-stabilized chaos, B-I blurs the distinction between deterministic and noise-mediated complexity. Both phenomena give emphasis to the dictum that the behavior of nonlinear systems often reflects the influence of non-stable, as well as stable, invariant sets – see [65, 70, 71] for examples and discussion.



**Figure 9.** Regions of bi-instability in relation to **a.** the  $\rho = 1/3$  and  $\rho = 1/4$  resonance horns and **b.** the  $\rho = 2/5$  and  $\rho = 2/7$  ultra-subharmonics. In **a.**, the rotation numbers are “unreduced,” *e.g.*,  $\rho = 2/6$  refers to period-doubled 3-cycles.



**Figure 10.** Supercritical period-doubling of the annual cycle gives way to subcritical period-doubling with increasing values of  $\beta_0$ . In the latter case, stable annual and biennial dynamics coexist. Compare with Figure 2 of [34]. The transition between these two dynamical regimes occurs at the co-dimension 2 bifurcation shown in Figure 8a, *i.e.*, where the curve labeled SN branches from PD-2. **a.**  $\beta_0 = 1500$ . **b.**  $\beta_0 = 2900$ .

**More Realistic Models.** As noted above, Equations (4) diverge from biological reality in a number of ways. Among the more egregious departures are the following:<sup>4</sup>

1. The assumption of linear transitions between **Exposed** and **Infectious** and **Infectious** and **Recovered** categories. This presumption results in exponential distributions for the latent and infectious periods, which intervals being bounded in nature, is clearly unrealistic [34, 35, 72].
2. The assumption that seasonality is adequately modeled by sines or cosines. Such functions fail [5, 6, 8] to capture the on-off character (“term-time forcing”) of the school year, which is generally held [4] to be the principal source of seasonal variation in contact.

Regarding these complications, we observe that their inclusion, while affecting the quantitative details of parametric dependence, has little effect on the overall pattern. Specifically, more realistic modeling [34, 35, 77] of latency and infectious periods, on the one hand, and seasonality [8], on the other, shift the bifurcation curves in Figure 8 to the left. This makes for better agreement between theory and observation, but does little to change the overall picture.

For example, in the course of studying a *SIR* model with realistic distributions of infectious periods, Lloyd [34, 35] observed the same change in criticality of the first period-doubling bifurcation predicted by Equations (4). The difference is that in Lloyd’s model the change occurs at lower values of  $\beta_0$  - compare our Figure 10, with his Figure 2 [34].

Similarly, Earn *et al.* [8], while retaining the assumption of exponentially distributed infectious periods, substitute term-time forcing for the cosine function in Equations (4). Still, their Figure 1 is qualitatively compatible with our analysis as summarized in Figure 8 – just follow a transect of increasing  $\beta_0$  for fixed  $\varepsilon_B$ .

As discussed in [78], Equations (4) are also consistent with the observation [8] that multiplying the production of **Susceptibles**, by increasing  $m$ , is destabilizing – again, the bifurcation curves are shifted left. To be fair, however, it is

---

<sup>4</sup> Other unrealistic assumptions include the following: **1.** The assumption of quadratic transmission kinetics, surely an over simplification given upper limits on the number of **Susceptibles** that a single infectious individual can contact [73, 74]. **2.** The assumption of homogeneity with regard to age [5-7] and space [67, 68, 75, 76], which neglects fact that exposure goes up when children first enter school and that people sort into villages, town and cities and, within cities, into neighborhoods. **3.** The exclusion of demographic stochasticity noted above – especially troubling given the small numbers of infected individuals that can obtain under Equations (4).

worth pointing out that the use of *any* constant population size model to predict the effects of changing birth rates in the real world is probably inappropriate. In nature, rates of reproduction and mortality are not locked together in equality as Equations (4) and their allies presume.

Preservation of the global, albeit shifted, dynamical picture also obtains when one varies the non-contact related parameters,  $a$  and  $g$ , and relaxes the assumption of permanent immunity [78].

**Origin of Parametric Uniqueness.** The most intriguing result presented here is the rightward march of CSRs (Figure 8) in the  $\varepsilon_B$  bifurcation diagrams as one increases the value of  $\beta_0$ . For values of  $\beta_0$  in excess of some critical minimum, a large, probably infinite, number of stable motions coexists with the MPD. For larger values of  $\beta_0$ , these motions move to the right and are incorporated into the main sequence with the consequent emergence of UPD. Does this observation have a general explanation? We suspect that it may.

In studies of two and three species predator-prey systems, King and Schaffer [19, 20] showed that the dynamical consequences of seasonality could be understood in terms of two limiting cases. The first is a Hamiltonian [79-81] limit,  $\mathcal{H}$  at which point, the system is conservative and satisfies canonical equations. Here, there is an infinite number of overlapping resonance horns, and everything depends on initial conditions. The second limit,  $\Gamma$ , is a curve (in the limit of zero seasonality, otherwise a surface) of periodically perturbed Hopf bifurcations [37, 82-84], on which each resonance horn is represented by a single point. Moving from  $\mathcal{H}$  to  $\Gamma$  thus corresponds to the emergence of UPD. Whether coincidence or consequence of some underlying generality, charting a transect of increasing values of  $\beta_0$  for fixed  $\varepsilon_B$  in Figure 8c is similar to increasing  $\log \alpha$  for fixed  $\log \eta$  in Figure 4 of [19] in the sense that resonances drop out sequentially in order of increasing rotation number.

In the present case, there is neither a Hamiltonian limit nor a Hopf bifurcation. There is however, a nearby (non-Hamiltonian) conservative system that obtains in the autonomous case as the small parameter

$$\varepsilon = \beta_0 i^* \rightarrow 0 \quad (9)$$

[10]. We speculate that the emergence of UPD documented above may prove explicable by reformulating Equations (4) as a perturbation of a more general model that admits to the existence of  $\mathcal{H}$  and  $\Gamma$ . Such an embedding would necessarily relax the assumption of constant population size, which fortuitously would also be a step in the direction of increased biological realism.

### Acknowledgements.

We thank Aaron King who helped write the software [18] and Shandelle Henson for useful discussion and encouragement. This study was supported by the Department of Ecology and Evolutionary Biology at the University of Arizona.

### References.

- [1] Guckenheimer, J. and Holmes, P., 1983, *Nonlinear Oscillations, Dynamical Systems and Bifurcations of Vector Fields*. (New York: Springer-Verlag).
- [2] Anderson, R. M. and May, R. M., 1979, Population biology of infectious diseases: I. *Nature*, **280**, 361-367.
- [3] Keymer, A., 1982, Tapeworm infections. Pp. 109-138. **In**, Anderson, R. M. (Ed.) *Population Dynamics of Infectious Diseases: Theory and Applications*. (London: Chapman and Hall).
- [4] Fine, P. E. M. and Clarkson, J. A., 1982. Measles in England and Wales. I: An analysis of factors underlying seasonal patterns. *Int. J. Epidemiol.*, **11**, 5-14.
- [5] Schenzle, D., 1984, An age-structured model of pre- and post-vaccination measles transmission. *IMA J. Math. Appl. Med. Biol.*, **1**, 169-191.
- [6] Bolker, B. M., 1993, Chaos and complexity in measles models. *IMA J. Math. Appl. Med. Biol.*, **10**, 83-95.
- [7] Bolker, B. M. and Grenfell, B. T., 1993, Chaos and biological complexity in measles dynamics. *Proc. R. Soc. Lond. B*, **251**, 75-81.
- [8] Earn, D. J. D., Rohani, P., Bolker, B. M. and Grenfell, B. T., 2000, A simple model for complex transitions in epidemics. *Science*, **287**, 667-670.
- [9] Anderson, R. M., 1982, Directly transmitted viral and bacterial infections in man. Pp. 1-37. **In**: Anderson, R. M. (ed.) *Population Dynamics of Infectious Diseases: Theory and Applications*. (London: Chapman and Hall).
- [10] Schwartz, I. B. and Smith, H. L., 1983, Infinite subharmonic bifurcations in an SEIR epidemic model. *J. Math. Biol.*, **18**, 233-253.
- [11] Aron, J. L. and Schwartz, I. B., 1984, Seasonality and period-doubling bifurcations in an epidemic model. *J. Theor. Biol.*, **110**, 665-679.
- [12] Schwartz, I. B., 1992, Small amplitude, long period outbreaks in seasonally

driven epidemic models. *J. Math. Biol.*, **30**, 473-491.

[13] Billings, L. and Schwartz, I. B., 2002, Exciting chaos with noise: unexpected dynamics in epidemic outbreaks. *J. Math. Biol.*, **44**, 31-48.

[14] Parker, T. S. and Chua, L. O., 1989, *Practical Numerical Algorithms for Chaotic Systems* (New York: Springer-Verlag).

[15] Rand, D. H. and Wilson, H. B., 1991, Chaotic stochasticity: a ubiquitous source of unpredictability in epidemic models. *Proc. R. Soc. Lond. B*, **246**, 179-184.

[16] Press, W. H., Teukolsky, S. A., Vetterling, W. T. and Flannery, B. P., 1992, *Numerical Recipes in FORTRAN* (New York: Cambridge Univ. Press).

[17] Kuznetsov, Y. A., 1995, *Elements of Applied Bifurcation theory*. (New York: Springer-Verlag).

[18] King, A. A., 1999, *Hamiltonian Limits and Subharmonic Resonance in Models of Population Fluctuations*. Ph. D. Thesis. University of Arizona, Tucson.

[19] King, A. A. and Schaffer, W. M. 1999. The rainbow bridge: Hamiltonian limits and resonance in predator-prey dynamics. *J. Math. Biol.*, **39**, 439-469.

[20] King, A. A. and Schaffer, W. M. 2001, The geometry of a population cycle: A mechanistic model of snowshoe hare demography. *Ecology*, **82**, 814-830.

[21] Khibnik, A. I., Kuznetsov, Y. A., Levitan, V. V. and Nikolaev, E. V., 1990-92, Interactive LOCAL BIFurcation Analyzer. Unpublished Manual to LOCBIF Version 2.

[22] Dietz, K., 1976, The incidence of infectious diseases under the influence of seasonal perturbations. *Lect. Notes. Biomath.*, **11**, 1-15.

[23] Li, M. Y. and Muldowney, J. S., 1995, Global stability for the SEIR model in epidemiology. *Math. Biosci.*, **125**, 155-164.

[24] Korobeinikov, A., 2004, Lyapunov functions and global properties for *SEIR* and *SEIS* epidemic models. *Math. Med. Biol.*, **21**, 75-83.

[25] Lajmanovich, A. and Yorke, J. A., 1976, A deterministic model for gonorrhea in a nonhomogenous population. *Math. Biosci.*, **28**, 221-236.

[26] Thompson, J. M. T. and Stewart, H. B., 2002, *Nonlinear Dynamics and Chaos* (West Sussex: John Wiley and Sons).

[27] Grebogi, C., Ott, E. and Yorke, J. A., 1983, Crises, sudden changes in chaotic attractors and transient chaos. *Physica D.*, **7**, 181-200.

- [28] Schaffer, W. M., Kendall, B. E., Tidd, C. W. and Olsen, L. F., 1993, Transient periodicity and episodic predictability in biological dynamics. *IMA J. Math. Appl. Med. Biol.*, **10**, 217-247.
- [29] Olsen, L. F., Truty, G. L. and Schaffer, W. M., 1988, A nonlinear dynamic study of six childhood diseases in Copenhagen, Denmark. *Theor. Pop. Biol.*, **33**, 344-380.
- [30] Sparrow, C. S., 1982, *The Lorenz Equations* (Berlin: Springer-Verlag).
- [31] Devaney, R. L., 1986, *An Introduction to Chaotic Dynamical Systems*. (Menlo Park: Benjamin/Cummings).
- [32] Yorke, J. A. and Yorke, E. D., 1979, Metastable chaos: the transition to sustained chaotic behavior in the Lorenz model. *J. Statist. Phys.*, **21**, 263-277.
- [33] London, W. A. and Yorke, J. A., 1973, Recurrent outbreaks of measles, chicken-pox and mumps. I: Seasonal variation in contact rates. *Amer. J. Epidem.*, **98**, 453-468.
- [34] Lloyd, A. L., 2001, Destabilization of epidemic models with the inclusion of realistic distributions of infectious periods. *Proc. R. Soc. Lond. B*, **268**, 985-993.
- [35] Lloyd, A. L., 2001, Realistic distributions of infectious persistence in epidemic models: Changing patterns of persistence. *Theor. Pop. Biol.*, **60**, 59-71.
- [36] Auerbach, D., Cvitanovic P., Eckmann, J.-P. and Procaccia, I., 1987, Exploring chaotic motion through periodic orbits. *Phys. Rev. Lett.*, **58**, 2387-2389.
- [37] Grebogi, C., Ott, E. and Yorke, J. A., 1987, Unstable periodic orbits and the dimension of chaotic attractors. *Phys. Rev. A.*, **36**, 3522-3525.
- [38] Cvitanovic, P., 1988, Invariant measurement of strange sets in terms of cycles. *Phys. Rev. Lett.*, **61**, 2729-2732.
- [39] Auerbach, D., 1989, Dynamical complexity of strange sets. Pp. 203-207. In: Abraham, N. B., *et al.* (eds.) *Measures of Complexity and Chaos*. (New York: Plenum Press).
- [40] Lathrop, D. P. and Kostelich, E. J., 1989, Characterization of an experimental strange attractor by periodic orbits. *Phys. Rev. A.*, **40**, 4028-4031.
- [41] Vance, W. N. and Ross, J., 1991. Bifurcation structures of periodically forced oscillators. *Chaos*, **1**, 445-453.
- [42] Ott, E., 1993, *Chaos in Dynamical Systems* (Cambridge: Cambridge Univ. Press).
- [43] Engbert, R. and Drepper, F. R., 1994, Qualitative analysis of unpredictability: a

case study from childhood epidemics. Pp. 204-215. **In**, Grasman, J. and G. van Straten (Eds.) *Predictability and Nonlinear Modelling in Natural Sciences and Economics*. (Dordrecht: Kluwer).

[44] Kuznetsov, A. and Piccardi, C., 1994, Bifurcation analysis of periodic *SEIR* and *SIR* models. *J. Math. Biol.*, **32**, 109-121.

[45] Greeman, J., Kamo, M. and Boots, M., 2004, External forcing of ecological and epidemiological systems: a resonance approach. *Physica D*, **190**, 136-151.

[46] Guckenheimer, J., Oster, G. and Ipaktchi, A., 1976, The dynamics of density dependent population models. *J. Math. Biol.*, **4**, 101-147.

[47] Arnol'd, V. I., 1983, *Geometrical Methods in the Theory of Ordinary Differential Equations*. (New York: Springer-Verlag).

[48] Glass, K., Xia, Y. and Grenfell, B. T., 2003, Interpreting time-series for continuous-time models – measles as a case study. *J. Theoret. Biol.*, **223**, 19-25.

[49] Soper, H. E., 1929, Interpretation of periodicity in disease prevalence. *J. R. Statist. Soc.*, **92**, 34-73.

[50] Dietz, K., 1975, Transmission and control of arbovirus diseases. Pp. 104-121. **In**, Ludwig, D. and K. L. Cook (Eds.) *Epidemiology*. (Philadelphia: SIAM Press).

[51] Stirzaker, D. R., 1975, A perturbation method for the stochastic recurrent epidemic. *J. Inst. Math. Applic.*, **15**, 135-160.

[52] Anderson, R. M. and May, R. M., 1979, Population biology of infectious diseases: I. *Nature*, **280**, 361-367.

[53] Yorke, J. A., Nathanson, N., Piagiani, G. and Martin, J., 1979, Seasonality and the requirements for perpetuation and eradication of viruses in populations. *Am. J. Epidem.*, **109**, 103-123.

[54] Anderson, R. M. and May, R. M., 1982, Directly transmitted infectious diseases: control by vaccination. *Science*, **215**, 451-454.

[55] Schaffer, W. M., 1985, Can nonlinear dynamics elucidate mechanisms in ecology and childhood epidemics? *IMA J. Math. Appl. Med. Biol.*, **2**, 221-252.

[56] Olsen, L. F. and Schaffer, W. M., 1990, Chaos vs. noisy periodicity: Alternative hypotheses for childhood epidemics. *Science*, **249**, 499-504.

[57] Drepper, F. R., Engbert, R. and Stollenwerk, N., 1994, Nonlinear time series analysis of empirical population dynamics. *Ecol. Modell.*, **75/76**, 171-181.

- [58] Rohani, P., Keeling, M. J. and Grenfell, B. T., 2002, The interplay between determinism and stochasticity in childhood diseases. *Amer. Natur.*, **159**, 469-481.
- [59] Blarer, A. and Dobelli, M., 1999, Resonance effects and outbreaks in ecological time series. *Ecol. Lett.*, **2**, 167-177.
- [60] Wiggins, S., 1988, *Global Bifurcations and Chaos* (New York: Springer-Verlag).
- [61] Kooi, B. W. and Boer, M. P., 2003, Chaotic behavior of a predator-prey system in the chemostat. *Dynam. Contin. Discr. Impuls. Syst. B*, **10**, 259-272.
- [62] Boer, M.P., Kooi, B.W. and Kooijman, S. A. L. M., 1998, Food chain dynamics in the chemostat. *Math. Biosci.*, **150**, 43-62.
- [63] Boer, M.P., Kooi, B.W. and Kooijman, S. A. L. M., 1999, Homoclinic and heteroclinic orbits in a tri-trophic food chain. *J. Math. Biol.*, **39**, 19-38.
- [64] Boer, M.P., Kooi, B.W. and Kooijman, S. A. L. M., 2001, Multiple attractors and boundary crises in a tri-trophic food chain. *Math. Biosci.*, **169**, 109-128.
- [65] Cushing, J. M., Costantino, R. F., Dennis, B., Desharnais, R. A. and Henson, S., 2002. *Chaos in Ecology: Experimental Nonlinear Dynamics*. (San Diego: Academic Press).
- [66] Bartlett, M. S., 1960, The critical community size for measles in the United States. *J. R. Statist. Soc. A.*, **123**, 37-44.
- [67] Cliff, A. D., Haggett, P., Ord, J. K. and Versey, G. R., 1981, *Spatial Diffusion*. (Cambridge: Cambridge University Press).
- [68] Cliff, A., Haggett, P. and Smallman-Raynor, M., 1993, *Measles. An Historical Geography of a Major Human Disease*. (Oxford: Blackwell Publ.).
- [69] Nassell, I. 1999, On the time to extinction in recurrent epidemics. *J. R. Statist. Soc. B*, **61**, 309-330.
- [70] Henson, S. M., Costantino, R. F., Cushing, J. M., Dennis, B. and Desharnais, R. A., 1999, Multiple attractors, saddles, and population dynamics in periodic habitats, *Bull. Math. Biol.*, **61**, 1121-1149.
- [71] King, A. A., Costantino, R. M., Cushing, J. M., Henson, S. M., Desharnais, R. A. and Dennis, B., 2003, Anatomy of a chaotic attractor: subtle model-predicted patterns revealed in population data, *Proc. Nat. Acad. Sci. USA.*, **101**, 408-413.
- [72] Grossman, Z., 1980, Oscillatory dynamics in a model of infectious diseases. *Theor. Pop. Biol.*, **18**, 204-243.

- [73] Heesterbeek, J. A. P. and Metz, J. A. J., 1993, The saturating contact rate in marriage and epidemic models. *J. Math. Biol.*, **31**, 529-539.
- [74] Li, G. and Zin, J., 2005, Global stability of an *SEI* epidemic model with general contact rate. *Chaos, Solitons and Fractals*, **23**, 997-1004.
- [75] Lloyd, A. L. and May, R. M., 1996, Spatial heterogeneity in epidemic models. *J. Theor. Biol.*, **179**, 1-11.
- [76] Lloyd, A. L. and Jansen, V. A., 2004, Spatiotemporal dynamics of epidemics: synchrony in metapopulation models. *Math. Biosci.*, **188**, 1-16.
- [77] Keeling, M. J. and Grenfell, B. T., 2002, Understanding the persistence of measles: reconciling theory, simulation and observation. *Proc. R. Soc. London B.*, **269**, 335-343.
- [78] Schaffer, W. M. and Bronnikova, T. V., 2007, Parametric dependence in model epidemics. II: Non-contact related parameters. *J. Biol. Dynam.* (In press).
- [79] Hènon, M., 1983, Numerical explorations of Hamiltonian systems. Pp. 53-170. **In**, Ioos, G., Helleman, R. H. and R. Stora (Eds.) *Chaotic Behavior of Deterministic Systems*. (Amsterdam North-Holland).
- [80] Lichtenberg, A. J. and Lieberman, M. A., 1992, *Regular and Chaotic Dynamics*. (New York: Springer-Verlag).
- [81] Tabor, M., 1989, *Chaos and Integrability in Nonlinear Systems* (New York: John Wiley).
- [82] Kath, W. L., 1981, Resonance in periodically perturbed Hopf bifurcation. *Stud. Appl. Math.*, **65**, 95-112.
- [83] Bajaj, A. K., 1986, Resonant parametric perturbations of the Hopf bifurcation. *J. Math. Anal. Appl.*, **115**, 214-234.
- [84] Rosenblatt, S. and Cohen, D. S., 1981, Periodically perturbed bifurcations – II. Hopf Bifurcation. *Stud. Appl. Math.*, **64**, 143-175.